PAPER

Check for updates

Enhancing the intracellular delivery of antisense oligonucleotides (ASO) : a comparative study of aptamer, vitamin E, and cholesterol ASO conjugates

Akilandeswari Ashwini Balachandran,[ab] Bal Hari Poudel, [iD] [ab] Kamal Rahimizadeh,[ab] Arpitha Chikkanna[ab] and Rakesh N. Veedu [iD] *[ab]

Antisense oligonucleotides (ASOs) have emerged as powerful tools for gene modulation; however, their clinical application is often hindered by inefficient intracellular delivery. Recent advances suggest that conjugation to biomolecules such as aptamers, lipids, or vitamins may enhance uptake and efficacy. This study investigates the potential of aptamer, vitamin E, and cholesterol-conjugated ASOs to improve delivery and functional activity in cancer cell models. The ASO PNAT524 was conjugated to two DNA aptamers—AS1411 and S2.2—via thiol and triethylene glycol (TEG) linkers, respectively. In parallel, PNAT524 was modified with vitamin E and cholesterol moieties. The conjugates were evaluated for cellular uptake, exon-skipping activity, and cytotoxicity in cancer cell lines. Fluorescence microscopy was used to determine subcellular localization. Aptamer conjugation (AS1411, S2.2) did not significantly enhance exon-skipping efficiency compared to unconjugated PNAT524, consistent with previous findings. In contrast, vitamin E and cholesterol conjugates demonstrated potent, dose-dependent exon-skipping activity and cytotoxic effects. Among all formulations, the cholesterol-conjugated ASO (524-Chol) showed the highest efficacy, with superior splice-modulating and cytotoxic outcomes. Fluorescence microscopy confirmed nuclear and cytoplasmic localization of lipid-conjugated ASOs. These findings indicate that aptamer conjugation provides minimal benefit for ASO delivery, while cholesterol and vitamin E conjugation significantly enhance intracellular delivery and therapeutic activity. The 524-Chol conjugate holds strong potential for adaptation in ASOs targeting EGFR and other oncogenes, representing a promising avenue for ASO-based cancer therapeutics.

Introduction

Antisense oligonucleotides (ASOs) are increasingly recognized for their therapeutic potential in a variety of diseases,[1,2] with several gaining regulatory approval in recent years. Despite their promise, ASO therapies are limited by delivery barriers due to their hydrophilicity and vulnerability to nuclease degradation. Strategies such as lipid conjugation—particularly with cholesterol and vitamin E—have gained traction as effective approaches to improve cellular uptake and bioavailability.

The use of antisense oligonucleotides (ASOs) to modulate gene expression has emerged as a promising therapeutic strategy for a variety of diseases.[3] To date, nine ASOs have received approval from both the FDA and EMA for therapeutic use.[4] Most of these ASOs are administered locally and contain chemical modifications that protect them from degradation. Many ASOs are currently under development, employing various strategies to enhance their bioavailability and effectiveness *in vivo*. Due to their hydrophilic nature and low affinity for cell membranes, an effective delivery system is crucial.[5] We previously reported splice-modulating ASOs that effectively induced exon skipping in the extracellular and tyrosine kinase domains of EGFR *in vitro*.[6] Since the ASO internalization was mediated by a transfection reagent *in vitro*, modification of these ASOs for self-internalization would be ideal for *in vivo* applications. To advance the development of self-internalizing splice-modulating antisense oligonucleotides (ASOs), the EGFR-targeting ASO PNAT524 was selected as the therapeutic backbone and conjugated with various biomolecules, including aptamers, vitamin E, and cholesterol.

The therapeutic efficacy of ASOs largely depends on their ability to overcome physiological barriers and be delivered into target cells. This can be achieved through chemical modifications, conjugation with biomolecules, and the use of nanocarriers.[7] Chemical modifications in the internucleotide linkage, sugar moiety, and nucleobases improve the stability and potency of ASOs.

Conjugation with biomolecules like antibodies, peptides, *N*-acetyl galactosamine (GalNAc), polyethylene glycol (PEG),

[a]Personalised Medicine Center, Murdoch University, Perth, Western Australia 6150, Australia. E-mail: R.Veedu@murdoch.edu.au

[b]Precision Nucleic Acid Therapeutics, Perron Institute for Neurological and Translational Science, Nedlands, Western Australia 6009, Australia

aptamers, α-tocopherol, and cholesterol enhance the intracellular delivery of ASOs.[8] Carriers for ASOs can include liposomes, metal nanoparticles, lipid nanoparticles, polymer nanoparticles, and extracellular vesicles such as exosomes and microvesicles.[9,10]

This article examines biomolecule-conjugated ASOs, focusing on aptamer, vitamin E, and cholesterol conjugations. Aptamers are chemical antibodies with unique three-dimensional structures, generated against specific proteins or cells, and possess high affinity and specificity for their targets. Vitamin E and cholesterol are natural lipid molecules that are easily taken up by cells. When selecting biomolecules for conjugation, the primary consideration is the target cell type for ASO delivery. Additionally, the folding of the aptamer-ASO conjugate and the type of linker used for conjugation are critical factors influencing the delivery and efficacy of ASOs in cells.

Aptamers targeting specific molecules like prostate-specific membrane antigen (PSMA), human epidermal growth factor receptor 2 (HER2), alpha V beta 3 integrin (αVβ3), mucin-1 (MUC-1), nucleolin (NCL), toll-like receptor 9 (TLR9), Axl, B cell-activating factor receptor (BAFF-R), cluster of differentiation 30 (CD30), and transferrin have been used to deliver various oligonucleotides, such as siRNA, shRNA, and miRNA, specifically into cancer cells.[11,12] In this article, the aptamers used for ASO conjugation are NCL-specific AS1411 and MUC1-specific S2.2.

AS1411, previously known as AGRO-100, is a 26-nucleotide G-rich DNA aptamer that binds to the cell surface protein nucleolin (NCL) and is internalized by the cells. Since its discovery, various conjugates using AS1411 have been developed and tested for cancer cell imaging and targeted therapy.

To date, AS1411 has been successfully conjugated with nanoparticles,[13] doxorubicin,[14] siRNA,[15] DNAzymes,[16] shRNA,[17] and miRNA[18] to facilitate the intracellular delivery of these molecules.

The AS1411 aptamer has also been used to deliver ASOs targeting luciferase[19] and galectin 1 gene[20] to specific cells.

MUC1 S1.3/2.2 is a 25-mer DNA aptamer that has high specificity and affinity towards Mucin 1 (MUC1).[21] The S2.2 aptamer has been conjugated so far with siRNA targeting green fluorescent protein (GFP),[22] miR-29b-loaded hybrid nanoparticles,[23] luciferase- and GFP-targeting caged siRNAs.[24]

The term "vitamin E" encompasses tocopherols, tocotrienols, and their derivatives.[25] And the predominant form of vitamin E in the human body is α-tocopherol. Its cellular uptake is facilitated by lipoprotein receptors, including low-density lipoprotein receptor-related protein (LRP), low-density lipoprotein receptor (LDLR), and high-density lipoprotein (HDL) particles.[26] As a result, conjugating oligonucleotides with α-tocopherol is highly effective for cellular delivery.

The α-tocopherol was successfully conjugated to siRNAs (Toc-siRNA) targeting apolipoprotein B (ApoB), beta-site amyloid precursor protein cleaving enzyme 1 (BACE1)[27,28] and caged siRNAs targeting luciferase and GFP.[29]

A 13-mer LNA ASO gapmer targeting ApoB, conjugated with α-tocopherol and unlocked nucleic acids (UNA),[30] and α-tocopherol-conjugated heteroduplex oligonucleotides (HDOs) were delivered effectively *in vivo*.[31]

The internalization of α-tocopherol-loaded polymeric nanoparticles carrying ASOs and their effects on proliferation and apoptosis were primarily observed in lung cancer cell lines, as opposed to fibroblasts.[32] Our group previously reported the conjugation of vitamin E to splice-modulating ASOs targeting exon 23 of the dystrophin gene, both with and without a disulfide linker. The study demonstrated that incorporating a linker between the ASO and vitamin E is crucial for enhancing the exon-skipping activity of the ASO.[33] It was observed that conjugating oligonucleotides with α-tocopherol leads to the formation of micelle-like structures, which are responsible for the internalization of the conjugate into cells.[34]

Cholesterol is a preferred biomolecule for conjugating with oligonucleotides. Several studies have explored cholesterol conjugation strategies for the intracellular delivery of siRNA.[35,36] A comprehensive review of cholesterol-conjugated siRNA is available in the literature.[37]

Incorporating cholesterol into oligonucleotides enhances their cellular uptake and promotes sequence-specific activity in cancer cells[38] and the cellular uptake of cholesterol-conjugated ASOs was found to be mediated through the LDL receptor.[39]

Conjugating a splice-modulating ASO with cholesterol-conjugated spermine proved effective, and the resulting complex showed reduced interaction with serum proteins.[40]

The placement of cholesterol on the ASO and the choice of linker are critical factors influencing the ASO's accumulation and effectiveness in specific cell types. *In vivo* studies evaluated linkers such as hexamethylene succinimide (HMS), triethylene glycol (TEG), dihexyldisulfide-triethylene glycol (C6SS-TEG), and propyl disulfide (C3SS) conjugated at the 5′ or 3′ end of the ASO. Results indicated that the TEG linker significantly enhanced the reduction of target mRNA levels. The HMS linker and 3′ cholesterol conjugation improved the accumulation of the ASO in the liver. Moreover, better release of the ASO from the conjugate markedly increased its impact on the target *m*RNA.[41] A comparative study investigated cholesterol conjugation at the 5′ or 3′ ends of ASOs *versus* conjugation at the gap region. The results showed that ASOs with cholesterol attached to the gap region were efficiently delivered to the liver. However, introducing cleavage of the phosphorothioate (PS) linkages in these ASOs could potentially enhance their activity.[42]

Cholesterol conjugation, along with various modifications, has proven effective in improving the cellular delivery of ASOs, making it a valuable strategy in therapeutic applications.[43,44]

We designed and evaluated aptamer-conjugated ASOs for targeted delivery, and to develop cholesterol- and vitamin E-conjugated ASOs to improve cellular uptake. Additionally, we investigated the self-internalization capabilities of these biomolecule-conjugated ASOs in cancer cells and assessed their cytotoxic effects to determine their potential as personalized cancer therapeutics.

Methodology

Biomolecule conjugated ASO design and synthesis

The antisense oligonucleotide PNAT524 was synthesized as a 2′-*O*-methyl phosphorothioate (2′-OMe PS) oligonucleotide. This

molecule was conjugated with various biomolecules to create a range of constructs. Specifically, the nucleolin-targeting aptamer AS1411 was attached to PNAT524 using a C6 thiol linker, resulting in the construct 524-S-S-AS1411. For MUC1-targeted delivery, the MUC1-specific aptamer S2.2 was linked to PNAT524 *via* a TEG linker to form 524-TEG-S2.2. Cholesterol and vitamin E were both conjugated to PNAT524 at the 5′ end; cholesterol was attached using a thiol linker to create 524-S-S-Chol, while vitamin E was linked similarly, producing 524-S-S-VitE. In a separate approach, cholesterol was directly conjugated to the 5′ end of PNAT524 without a linker. Additionally, a scrambled version of PNAT524, which is the reverse complement of the original sequence, was synthesized as a 2′-OMe PS oligonucleotide and conjugated with cholesterol at the 5′ end *via* a thiol linker, resulting in SCR-S-S-Chol. All these sequences were commercially synthesized, desalted, purified, and characterized by SynGenis Pty Ltd, with detailed sequences provided in Table 1.

Cell lines

The MDA-MB-231 cell line was sourced from the American Type Culture Collection (ATCC) and was maintained in Dulbecco's Modified Eagle's Medium (DMEM) supplemented with 10% fetal bovine serum (FBS). U251-MG cells were procured from Cell Bank Australia and were cultured in Eagle's Minimal Essential Medium (EMEM) with 10% FBS. Both cell types were incubated at 37 °C in a 5% CO_2 environment.

AS1411 PNAT524 conjugate treatment

To prepare the 524-S-S-AS1411 conjugate, it was diluted to a 100 μM concentration in 2X PBS. The solution was then subjected to denaturation at 95 °C for 5 minutes, followed by a gradual cooling to room temperature. Upon reaching 80% confluency, MDA-MB-231 and U251-MG cells were subcultured and counted. These cells were resuspended in OptiMEM and aliquoted into separate tubes, each containing 40 000 cells. Different volumes of the denatured and annealed 524-S-S-AS1411 conjugate were added to achieve final concentrations of 0.5 μM, 1.0 μM, 2.5 μM, and 5.0 μM. The prepared cell suspensions with the conjugate were then plated into individual wells of 24-well plates and incubated for a duration of 4 days.

S2.2 PNAT524 conjugate treatment

Upon reaching 80% confluency, MDA-MB-231 cells were subcultured, counted, and plated into 24-well plates at a density of 40 000 cells per well in growth media. Prior to transfection, the 524-TEG-S2.2 conjugate was prepared by diluting it to a 100 μM concentration using 2X PBS. The diluted conjugate was then denatured at 95 °C for 5 minutes and subsequently allowed to cool to room temperature. Following this, different volumes of the denatured 524-TEG-S2.2 were added to the wells containing incomplete DMEM to achieve final concentrations of 0.5 μM, 1.0 μM, 2.5 μM, and 5.0 μM. The cells were harvested for analysis at 1, 2, 3, 5, and 7 days post-transfection with the 524-TEG-S2.2 conjugate.

Vitamin E and cholesterol-conjugated PNAT524 treatment

Once MDA-MB-231 cells reached 80% confluency, they were subcultured, counted, and plated at a density of 40 000 cells per well in 24-well plates using growth media. After allowing the cells to acclimate for 24 hours, vitamin E and cholesterol conjugated ASO were introduced directly into the wells using incomplete DMEM. The experiment was designed as a dose–response study, testing concentrations of 0.5 μM, 1 μM, 2.5 μM, and 5 μM.

PNAT524 lipofectamine transfection

According to the manufacturer's instructions, 100 nM of PNAT524 was used as positive control and transfected into the cells with Lipofectamine 3000 (ThermoFisher Scientific; Cat# L3000015). Additionally, PNAT524 was incubated directly with the cells in incomplete DMEM to investigate its direct uptake by the cells.

RNA extraction and PCR

After treatment with the ASO conjugates, cells were collected and lysed using the lysis buffer from the ISOLATE II RNA Mini Kit (Bioline; Cat# BIO-52073). RNA extraction was performed according to the manufacturer's guidelines, and RT-PCR was carried out using 50 ng of total RNA. The PCR was conducted with EGFR primers designed to amplify transcripts from exons 1 through 4 and GAPDH primers (as detailed in Table 2) using the SuperScript III One-Step RT-PCR Kit (ThermoFisher Scientific; Cat# 12574026). The conditions for PCR amplification are

Table 1 Sequence detail used in this study. * – Phosphorothioate backbone

ASO name	Sequence (3′-5′)
PNAT524	mA*mC*mC*mA*mG*mC*mC*mA*mC*mC*mU*mC*mC*mU*mG*mG*mA*mU*mG*mG*mU* mC*mU*mA*mA
524-S-S-AS1411	FAM/mA*mC*mC*mA*mG*mC*mC*mA*mC*mC*mU*mC*mC*mU*mG*mG*mA*mU*mG*mG*mU*mC*mU*mA*mA*/Thiol C6 S-S/dGdGdTdGdGdTdGdGdTdGdGdTdTdGdTdGdGdTdGdGdTdGdGdTdGdG/Cy3
524-TEG-S2.2	FAM/mA*mC*mC*mA*mG*mC*mC*mA*mC*mC*mU*mC*mC*mU*mG*mG*mA*mU*mG*mG*mU*mC*mU*mA*mA/TEG/dGdCdAdGdTdTdGdAdTdCdCdTdTdTdGdGdAdTdAdCdCdCdTdGdG/Cy3/
524-S-S-VitE	FAM/mA*mC*mC*mA*mG*mC*mC*mA*mC*mC*mU*mC*mC*mU*mG*mG*mA*mU*mG*mG*mU* mC*mU*mA*mA*/Thiol C6 S-S/VitE
524-S-S-chol	FAM/mA*mC*mC*mA*mG*mC*mC*mA*mC*mC*mU*mC*mC*mU*mG*mG*mA*mU*mG*mG*mU* mC*mU*mA*mA*/Thiol C6 S-S/Cholesterol
524-Chol	FAM/mA*mC*mC*mA*mG*mC*mC*mA*mC*mC*mU*mC*mC*mU*mG*mG*mA*mU*mG*mG*mU*mC*mU*mA*mA/Cholesterol
SCR-S-S-chol	mU*mU*mA*mG*mA*mC*mC*mA*mU*mC*mC*mA*mG*mG*mA*mG*mG*mU*mG*mG*mC*mU*mG*mG*mU-S-S/Cholesterol

specified in Tables 3 and 4. The resulting PCR products were subjected to electrophoresis on a 2% agarose gel prepared with tris-acetate-EDTA (TAE) buffer. Post-electrophoresis, the gels were stained with Red Safe (iNtRON Biotechnology; Cat# 21141) and then destained with deionised water. Gel images were captured using the Fusion FX gel documentation system (Vilber Lourmat, Marne La Vallée, France). Densitometric analysis of the bands was conducted using Image J software.

Cell viability assay

MDA-MB-231 cells, once reaching 80% confluency, were sub-cultured, counted, and plated onto 96-well plates at a density of 6000 cells per well in growth media. After 24 hours, various ASO conjugates were added to the cells in incomplete DMEM. To assess cell viability, concentrations of 0.5 µM, 1 µM, 2.5 µM, and 5 µM of the conjugates were tested. Five days post-transfection, 10 µl of the WST-1 cell proliferation reagent (Roche; Cat# 11644807001) was introduced to each well. The plates were then incubated for 1 hour at 37 °C in a 5% CO_2 humidified incubator. Absorbance was recorded at 450 nm using the FLUOstar Omega microplate reader (BMG Labtech). The percentage of cell viability was determined by comparingthe absorbance of treated cells to that of untreated controls.

Microscopic studies

Upon reaching 80% confluency, MDA-MB-231 cells were sub-cultured, counted, and seeded onto 24-well plates that had been pre-coated with 50 µg mL^{-1} of poly-D-lysine hydrobromide (Sigma-Aldrich; Cat# P1024). The cells were plated at a density of 40 000 cells per well in growth media. After 24 hours, fluorescein 45-labeled ASO conjugates, including 524-S-S-Chol, 524-S-S-VitE, and 524-Chol, were added to the cells in incomplete DMEM at final concentrations of 1 µM and 2.5 µM. Following a 48-hours incubation period, nuclei staining was performed using Hoechst (Invitrogen; Cat# H3570) for 10 minutes. The cells were then washed three times with 20% FBS in phosphate-buffered saline (PBS). Imaging was carried out using the Olympus TS-100 inverted fluorescence microscope.ain paragraph text follows directly on here.

Results

Biomolecule ASO conjugate design

Fig. 1 illustrates the biomolecule-conjugated ASOs utilized in this study. PNAT524 was synthesized as a 2′-OMe PS ASO (Fig. 1A). Conjugation to the 3′ end of PNAT524 involved the AS1411 aptamer, vitamin E, and cholesterol using a thiol linker (Fig. 1B, D and E) (designated as 524-S-S-AS1411, 524-S-S-VitE,

Table 2 Primers used for EGFR and GAPDH amplification

Primer name	Sequence 5′–3′	Amplicon size
hEGFR_1 Ex1F	CGGGCTCTGGAGGAAAAGAAAG	457bp
hEGFR_1 Ex4R	TGCTGAGAAAGTCACTGCTGA	
GAPDH-fwd	GGACTCATGACCACAGTCCATGC	492bp
GAPDH-rev	TTACTCCTTGGAGGCCATGTGGG	

Table 3 PCR conditions for EGFR amplification

Temp	Time	Cycles
55 °C	30 minutes	
94 °C	2 minutes	
94 °C	30 seconds	30
55 °C	1 minute	
68 °C	2 minutes	

and 524-S-S-Chol, respectively). In addition, the S2.2 aptamer was conjugated to the 3′ end of PNAT524 via a TEG linker (Fig. 1C) (identified as 524-TEG-S2.2). To investigate the role of the thiol linker, another cholesterol conjugate without this linker was designed (Fig. 1F) (referred to as 524-Chol). A scrambled control, created using the reverse complement sequence of PNAT524 and conjugated with cholesterol via a thiol linker (SCR-S-S-Chol), was also included. The 5′ end of 524-S-S-AS1411, 524-TEG-S2.2, 524-S-S-VitE, 524-S-S-Chol, and 524-Chol was tagged with FAM fluorescent dye, while the 3′ end of 524-S-S-AS1411 and 524-TEG-S2.2 were tagged with Cy3. The dual fluorophore labelling in the aptamer-ASO conjugates was incorporated to facilitate the study of intracellular localization.

Exon skipping activity of AS1411 PNAT524 conjugate

The denatured and annealed aptamer-ASO conjugate 524-S-S-AS1411 was used for reverse transfection in MDA-MB-231 and U251-MG cells. These cell lines were selected due to their high levels of exon 3 skipping (>80%) observed with PNAT524 transfection.[6] After a 4-days treatment period, RNA was extracted from the treated cells and amplified using primers specific to EGFR exons 1–4. Gel electrophoresis of the PCR products revealed full-length EGFR bands, with a clear exon 3-skipped band seen in cells treated with Lipofectamine-transfected PNAT524 at a concentration of 100 nM. Conversely, a faint exon 3-skipped band was detected at higher concentrations of 524-S-S-AS1411 in MDA-MB-231 cells but was not observed in U251-MG cells (Fig. 2A).

To investigate the poor exon-skipping activity, the experiment was adjusted by varying the salt concentration during the dena-turation and annealing of the conjugate. This modification did not improve the exon-skipping activity. Therefore, the secondary structure of the conjugate was analyzed using the Mfold online tool.[45] Since linkers could not be included in the sequence, the PNAT524 and AS1411 sequences were analyzed together. The predicted secondary structures for all three configurations showed significant intramolecular interactions between AS1411

Table 4 PCR conditions for GAPDH amplification

| Temp	Time	Cycles
55 °C	30 minutes	
94 °C	2 minutes	
94 °C	30 seconds	25
60 °C	1 minute	
68 °C	2 minutes	
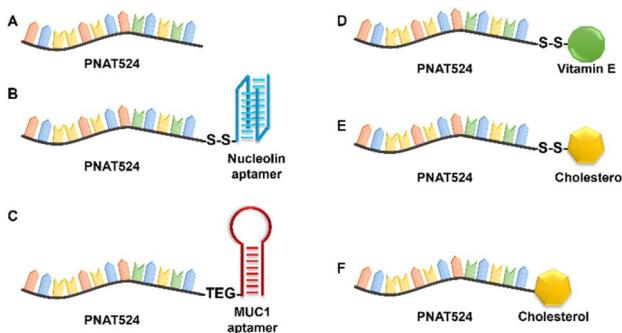
Fig. 1 A graphical representation of unconjugated and biomolecule conjugated ASOs. (A) PNAT524, (B) 524-S-S-AS1411, (C) 524-TEG-S2.2, (D) 524-S-S-VitE, (E) 524-S-S-Chol, and (F) 524-Chol.
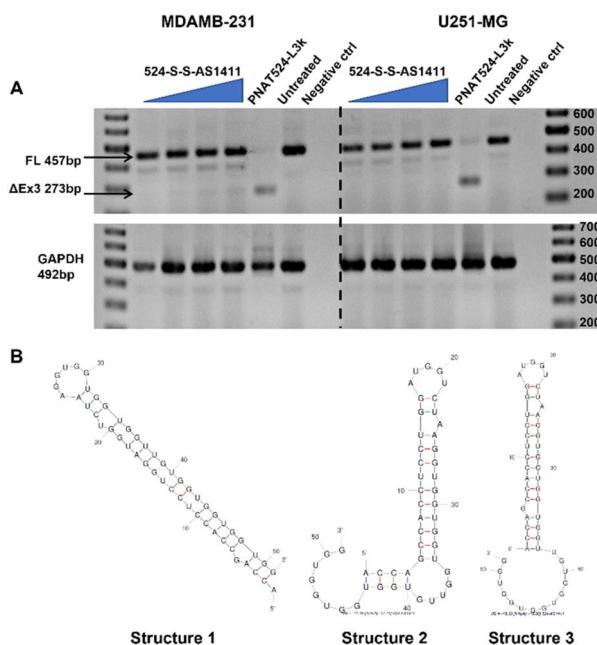

Fig. 2 AS1411 PNAT524 conjugate evaluation and predicted structure (A) RT-PCR analysis of 524-S-S-AS1411 exon skipping activity at 0.5, 1.0, 2.5 and 5 μM concentrations in MDA-MB-231 and U251-MG cells after 4 days of treatment and (B) Mfold predicted secondary structures of 524-S-S-AS1411 conjugate.

and PNAT524 (Fig. 2B). These interactions might contribute to the observed suboptimal exon-skipping activity of the conjugate.

Exon skipping activity of S2.2 PNAT524 conjugate

Prior to synthesis, the secondary structure of the 524-TEG-S2.2 conjugate was predicted using the Mfold software. The analysis identified two potential structures, in which the aptamer (S2.2) and the antisense oligonucleotide (ASO) PNAT524 remained separately folded, without interfering with each other (Fig. 3A). This prediction suggested that the S2.2 aptamer would maintain its native conformation, minimizing intramolecular interactions with PNAT524.

The denatured and annealed 524-TEG-S2.2 conjugate was directly transfected into MDA-MB-231 cells, with samples collected at intervals of 1, 2, 3, 5, and 7 days post-treatment.

RNA extracted from these treated cells was subjected to RT-PCR using primers specific to EGFR exon 1–4. Agarose gel electrophoresis of the PCR products revealed full-length EGFR transcript bands, with a faint exon 3-skipped band appearing in cells treated with 524-TEG-S2.2 after three days (Fig. 3B). In comparison, stronger exon 3 skipping was observed in cells transfected with the L3k form of PNAT524.

To evaluate the possibility of self-internalization of PNAT524, gymnotic uptake with 2.5 μM and 5 μM concentrations of PNAT524 were included in the 5- and 7-days treatments. Results from agarose gel electrophoresis demonstrated the presence of both full-length and exon 3-skipped bands across all samples. Interestingly, unconjugated PNAT524 exhibited exon-skipping activity comparable to that observed with 524-TEG-S2.2 treatment (Fig. 3C). As there was limited improvement in exon-skipping observed beyond five days, the study standardized on a five-day treatment protocol, maintaining the same concentrations for unconjugated PNAT524 gymnotic uptake as used for the 524-TEG-S2.2 conjugate.

Dose-dependent exon skipping activity of S2.2 PNAT524 conjugate

The evaluation of exon-skipping activity for the 524-TEG-S2.2 conjugate and PNAT524 in MDA-MB-231 cells revealed distinct outcomes. A dose study was conducted to compare the effectiveness of these treatments. Agarose gel electrophoresis results showed no dose-dependent exon skipping with the 524-TEG-S2.2
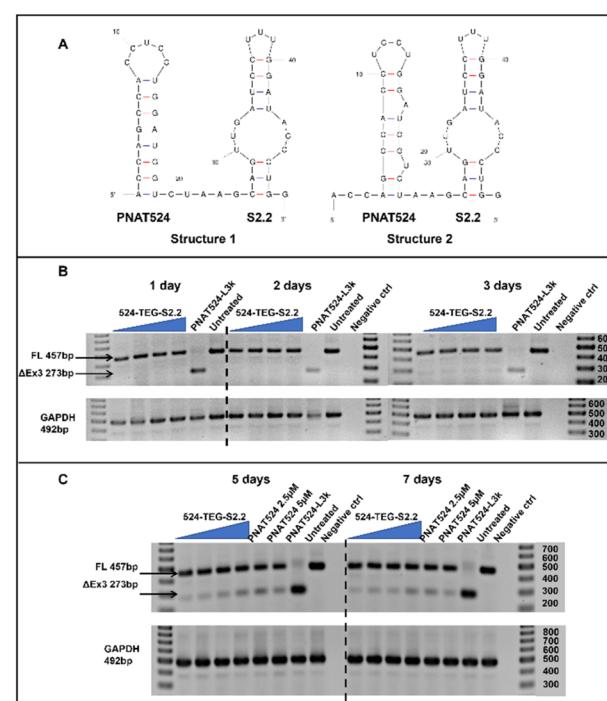
Fig. 3 S2.2 PNAT524 conjugate predicted structure and evaluation (A) Mfold predicted secondary structures of 524-TEG-S2.2 conjugate (B) RT-PCR analysis of 524-TEG-S2.2 exon skipping activity at 0.5, 1.0, 2.5, and 5 μM concentrations after 1, 2, and 3 days of treatment in MDA-MB-231 cells (C)) RT-PCR analysis of 524-TEG-S2.2 exon skipping activity at 0.5, 1.0, 2.5, and 5 μM concentrations after 5 and 7 days of treatment in MDA-MB-231 cells.

conjugate. In contrast, gymnotic uptake of PNAT524 demonstrated a clear dose-dependent exon-skipping effect. Densitometry analysis quantified this, revealing 51.2% exon skipping with 5 μM PNAT524 gymnosis, while 5 μM 524-TEG-S2.2 treatment resulted in 40.6% exon skipping (Fig. 4). These findings indicate that the 524-TEG-S2.2 conjugate did not effectively internalize through the MUC1 aptamer as intended.

Dose-dependent exon skipping activity of vitamin E and cholesterol conjugated ASOs

The exon-skipping activity of vitamin E and cholesterol-conjugated ASOs was initially evaluated at 0.5 and 1 μM concentrations, revealing dose-dependent exon-skipping effects. To further explore these findings, a dose study was conducted with 524-S-S-VitE, 524-S-S-Chol, 524-Chol, and SCR-S-S-Chol conjugates over a 5-days treatment period. Agarose gel electrophoresis demonstrated dose-dependent exon-skipping activity across all 524 conjugates, while the scrambled CR-S-S-Chol conjugate showed no exon-skipping. Densitometry analysis quantified exon skipping at 86.5% for 524-S-S-VitE, 83.4% for 524-S-S-Chol, and 93.6% for 524-Chol (Fig. 5 and 6). Notably, the cholesterol-conjugated ASO without a linker (524-Chol) exhibited superior exon-skipping performance compared to the cholesterol conjugate with a thiol linker (524-S-S-Chol).

Cytotoxicity of conjugates

The cytotoxic effects of the ASO conjugates on MDA-MB-231 breast cancer cells were assessed using the WST assay. This

analysis was conducted with 0.5, 1.0, 2.5, and 5 μM concentrations of the ASO conjugates over 4 and 5 days. The results indicated that all ASO conjugates exhibited dose-dependent cytotoxicity. After 4 days, the cell viability was significantly reduced with the 524-Chol conjugate, showing only 45.8% viability at 5 μM compared to untreated cells (100%). For the same concentration, 524-S-S-Chol, 524-S-S-VitE, and SCR-S-S-Chol showed viabilities of 51.2%, 59.2%, and 59.5%, respectively (Fig. 7A). In contrast, gymnotic uptake of naked PNAT524 did not exhibit any dose-dependent cytotoxic effects. After 5 days of treatment with ASO conjugates, cell viability dropped to 40.7% and 51.9% in cells treated with 524-Chol conjugate. This decline was not observed with the other conjugates. In contrast, cells treated with 524-S-S-Chol and 524-S-S-VitE showed viabilities of 60.3% and 66.6%, respectively (Fig. 7B).

Cellular internalization of conjugates

Fluorescent microscopic images of MDA-MB-231 cells were obtained after 2 days of treatment with 524-S-S-VitE, 524-S-S-Chol, and 524-Chol conjugates. Overlaying the FAM and Hoechst channels revealed that all conjugates localized to both the cytoplasm and nucleus (Fig. 8). The red arrows in the images highlight the nuclear localization of the conjugates. These images represent cells treated with 2.5 μM of each ASO conjugate.

Discussion

In this study, we systematically evaluated three biomolecule-based conjugation strategies—aptamers (AS1411 and S2.2), vitamin E, and cholesterol—to enhance the intracellular
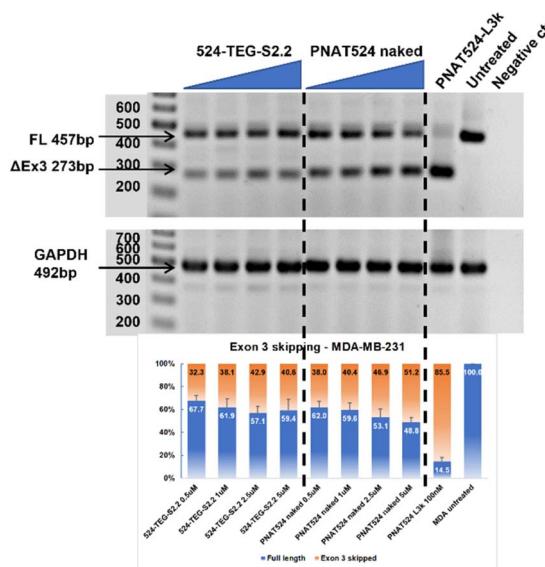

Fig. 4 RT–PCR and densitometry analysis of exon skipping activity of 524-TEG-S2.2 conjugate. Agarose gel showing exon skipping following 524-TEG-S2.2 conjugate and PNAT524 naked transfection in MDA-MB-231 cells. The dose concentrations were 0.5, 1.0, 2.5, and 5 μM, and as a positive control, PNAT524 was transfected at 100 nM concentration. Densitometry graph of percentage exon skipping is shown, and data are represented as mean ± SEM.
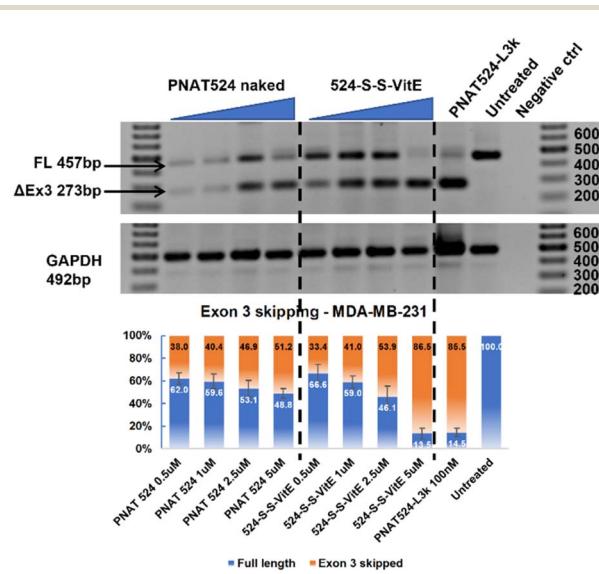

Fig. 5 RT–PCR and densitometry analysis of exon skipping activity of 524-S-S-VitE conjugate. Agarose gel showing exon skipping following 524-S-S-VitE conjugate and PNAT524 naked transfection in MDA-MB-231 cells. The dose concentrations were 0.5, 1.0, 2.5, and 5 μM, and as a positive control, PNAT524 was transfected at 100 nM concentration. Densitometry graph of percentage exon skipping is shown, and data are represented as mean ± SEM.
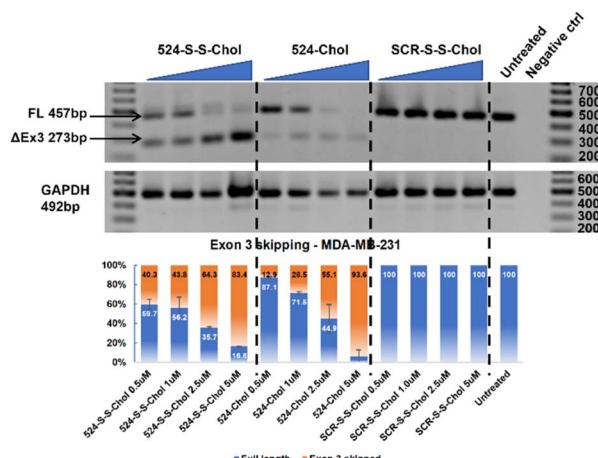
Fig. 6 RT-PCR and densitometry analysis of exon skipping activity of cholesterol conjugated ASOs. Agarose gel showing dose-dependent exon skipping following 524-S-S-Chol and 524-Chol conjugate treatment and no exon skipping with SCR-S-S-Chol naked transfection in MDA-MB-231 cells. The dose concentrations were 0.5, 1.0, 2.5, and 5 μM. Densitometry graph of percentage exon skipping is shown, and data are represented as mean ± SEM.
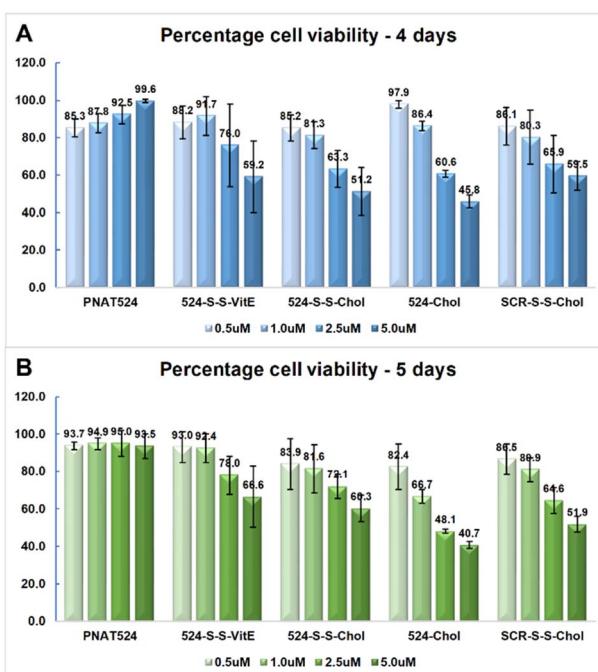

Fig. 7 Cytotoxicity of ASO conjugates in MDA-MB-231 cells. Percentage cell viability of MDA-MB-231 cells after (A) 4 days and (B) 5 days of treatment with ASO conjugates and PNAT524.

delivery and therapeutic efficacy of splice-modulating antisense oligonucleotides (ASOs) in cancer cells. Although aptamers are frequently employed in targeted delivery strategies due to their high specificity and affinity toward cell surface receptors,[46,47] their utility in enhancing ASO delivery remains limited, as evidenced by our findings.
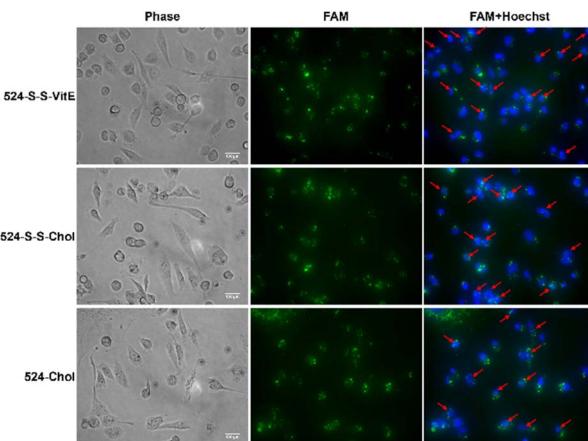
Fig. 8 Fluorescent microscopic images of MDA-MB-231 cells treated with 524-S-S-VitE, 524-S-S-Chol, and 524-Chol conjugates.

The conjugation of AS1411 to PNAT524 did not significantly improve exon-skipping activity. Computational analysis revealed potential intramolecular interactions between the ASO and the aptamer that could hinder the release and function of the therapeutic oligonucleotide. This limitation aligns with other reports suggesting that improper folding or strong secondary structures in conjugated aptamers can impede cargo release.[12] Similarly, the S2.2 aptamer, despite being structurally independent when analyzed *in silico*, failed to demonstrate improved ASO activity or cellular uptake. This indicates that preservation of aptamer structure alone may not be sufficient for functional delivery, as receptor-mediated internalization pathways might not be effectively triggered.[48] Both the aptamer conjugates were denatured and gradually annealed, which is recommended for efficient aptamer binding in cell-based assays. This process is also important for aptamer tertiary structure formation resulting in improved specificity and affinity for target protein.[46] The AS1411 aptamer is bound to cell surface nucleolin and internalized into the cells by micropinocytosis. In order to facilitate better uptake, the 524-S-S-AS1411 aptamer conjugate was treated using reverse transfection method.[47]

Conversely, both vitamin E and cholesterol conjugation significantly enhanced the delivery and functionality of PNAT524. The vitamin E-conjugated ASO (524-S-S-VitE) demonstrated robust exon-skipping and cytotoxic effects, consistent with previous reports highlighting the utility of α-tocopherol in facilitating lipoprotein receptor-mediated uptake.[26,31] Moreover, the cholesterol conjugates, particularly 524-Chol, exhibited superior performance among all formulations tested. This cholesterol-mediated enhancement corroborates existing literature suggesting that cholesterol improves ASO delivery *via* LDL receptor pathways and enhances serum protein binding, thereby stabilizing oligonucleotides in circulation.[41,42]

Interestingly, our findings also suggest that linker chemistry plays a pivotal role in modulating ASO efficacy. The 524-Chol conjugate, synthesized without a linker, performed better than its

thiol-linked counterpart (524-S-S-Chol), potentially due to increased release efficiency or altered uptake mechanisms. This observation aligns with recent insights that fine-tuning linker composition and conjugation sites can significantly influence tissue tropism, endosomal escape, and ASO release dynamics.[41,44]

Previous studies suggest that cholesterol conjugates ASOs might form micelles or spherical vesicles based on the length of ASO and linker used.[48] A detailed physicochemical characterization of cholesterol and vitamin E conjugated ASOs will be important to understand the colloidal properties and in turn elucidate cellular internalization of these conjugates.

Overall, our results position cholesterol conjugation as the most effective strategy for enhancing ASO delivery to cancer cells. This approach may be particularly promising for therapeutic applications targeting EGFR and other overexpressed oncogenes in cancers such as breast, glioblastoma, and hepatocellular carcinoma. This study would benefit from a comprehensive analysis of cellular internalization and uptake of these conjugates to further substantiate their role in enhancing targeted delivery. Future studies should expand on this work by exploring combinatorial linker and lipid designs, testing *in vivo* efficacy, and evaluating biodistribution and toxicity in animal models.

Conclusions

This study reveals that cholesterol conjugation is a superior strategy for improving the intracellular delivery and functional efficacy of antisense oligonucleotides in cancer cells. While aptamer-based delivery approaches remain theoretically attractive, their current implementations show limited enhancement in ASO efficacy. Vitamin E conjugation also offers a viable alternative; however, it falls short of the performance observed with cholesterol-conjugated ASOs. Among the tested strategies, the 524-Chol conjugate emerged as the most potent, demonstrating strong exon-skipping activity, less cytotoxic effects, and efficient internalization. These findings support the further development of cholesterol-conjugated ASOs for targeted cancer therapeutics and underscore the importance of rational design in conjugate chemistry.

Author contributions

A. A. B., K. R., and R. N. V. designed the experiments, A. A. B., K. R., and A. C. conducted experiments. A. A. B. and B. H. P. wrote the manuscript. A. A. B., K. R., A. C., B. H. P. and R. N. V. revised the manuscript.

Conflicts of interest

There are no conflicts to declare.

Data availability

All data supporting the findings of this study are included within the article. Additional details are available from the corresponding author upon request.

Supplementary information: experimental and spectral data, and crystallographic data. See DOI: https://doi.org/10.1039/d5ra05904f.

Acknowledgements

References

1 T. Rogers, Antisense oligonucleotides: Navigating ethical and safety challenges, *Drug Discovery World*, 2025, vol. 26(1), https://www.ddw-online.com/antisense-oligonucleotides-navigating-ethical-and-safety-challenges-33473-202502/.

2 M. C. Lauffer, *et al.*, Possibilities and limitations of antisense oligonucleotide therapies for the treatment of monogenic disorders, *Commun. Med.*, 2024, **4**(1), 6.

3 S. Thakur, *et al.*, A perspective on oligonucleotide therapy: Approaches to patient customization, *Front. Pharmacol*, 2022, **13**, 1006304.

4 J. M. Migliorati, *et al.*, Absorption, Distribution, Metabolism, and Excretion of US Food and Drug Administration-Approved Antisense Oligonucleotide Drugs, *Drug Metab. Dispos.*, 2022, **50**(6), 888–897.

5 M. Raouane, *et al.*, Lipid conjugated oligonucleotides: a useful strategy for delivery, *Bioconjug. Chem.*, 2012, **23**(6), 1091–1104.

6 A. A. Balachandran, *et al.*, Splice-Switching Antisense Oligonucleotides Targeting Extra- and Intracellular Domains of Epidermal Growth Factor Receptor in Cancer Cells, *Biomedicines*, 2023, **11**(12), 3299.

7 M. Gagliardi and A. T. Ashizawa, The Challenges and Strategies of Antisense Oligonucleotide Drug Delivery, *Biomedicines*, 2021, **9**(4), 433.

8 T. C. Roberts, R. Langer and M. J. A. Wood, Advances in oligonucleotide drug delivery, *Nat. Rev. Drug Discov.*, 2020, **19**(10), 673–694.

9 L. Goldbloom-Helzner, *et al.*, Assessing the conjugation efficiency of surface-modified extracellular vesicles using single nanovesicle analysis technologies, *Nanoscale*, 2024, **16**(45), 20903–20916.

10 R. Gupta, *et al.*, Versatility of Liposomes for Antisense Oligonucleotide Delivery: A Special Focus on Various Therapeutic Areas, *Pharmaceutics*, 2023, **15**(5), 1435.

11 K. W. Thiel and P. H. Giangrande, Intracellular delivery of RNA-based therapeutics using aptamers, *Ther. Deliv.*, 2010, **1**(6), 849–861.

12 J. P. Dassie and P. H. Giangrande, Current progress on aptamer-targeted oligonucleotide therapeutics, *Ther. Deliv.*, 2013, **4**(12), 1527–1546.

13 R. Yazdian-Robati, *et al.*, Therapeutic applications of AS1411 aptamer, an update review, *Int. J. Biol. Macromol.*, 2020, **155**, 1420–1431.

14 H. Xing, *et al.*, Selective Delivery of an Anticancer Drug with Aptamer-Functionalized Liposomes to Breast Cancer Cells in Vitro and in Vivo, *J. Mater. Chem. B*, 2013, **1**(39), 5288–5297.

15 L. Li, *et al.*, Nucleolin-targeting liposomes guided by aptamer AS1411 for the delivery of siRNA for the treatment of malignant melanomas, *Biomaterials*, 2014, **35**(12), 3840–3850.

16 N. Subramanian, *et al.*, Chimeric nucleolin aptamer with survivin DNAzyme for cancer cell targeted delivery, *Chem. Commun.*, 2015, **51**(32), 6940–6943.

17 S. Ayatollahi, *et al.*, Aptamer-targeted delivery of Bcl-xL shRNA using alkyl modified PAMAM dendrimers into lung cancer cells, *Int. J. Biochem. Cell Biol.*, 2017, **92**, 210–217.

18 P. Daei, *et al.*, Aptamer-based Targeted Delivery of miRNA let-7d to Gastric Cancer Cells as a Novel Anti-Tumor Therapeutic Agent, *Iran. J. Pharm. Res.*, 2018, **17**(4), 1537–1549.

19 J. W. Kotula, *et al.*, Aptamer-mediated delivery of splice-switching oligonucleotides to the nuclei of cancer cells, *Nucleic Acid Ther.*, 2012, **22**(3), 187–195.

20 S. Hong, *et al.*, Building a chimera of aptamer–antisense oligonucleotide for silencing galectin-1 gene, *RSC Adv.*, 2016, **6**(113), 112445–112450.

21 C. S. Ferreira, C. S. Matthews and S. Missailidis, DNA aptamers that bind to MUC1 tumour marker: design and characterization of MUC1-binding single-stranded DNA aptamers, *Tumor Biol.*, 2006, **27**(6), 289–301.

22 H. Yoo, *et al.*, Multivalent comb-type aptamer-siRNA conjugates for efficient and selective intracellular delivery, *Chem. Commun.*, 2014, **50**(51), 6765–6767.

23 M. Perepelyuk, *et al.*, Evaluation of MUC1-Aptamer Functionalized Hybrid Nanoparticles for Targeted Delivery of miRNA-29b to Nonsmall Cell Lung Cancer, *Mol. Pharm.*, 2018, **15**(3), 985–993.

24 L. Zhang, *et al.*, Photomodulating Gene Expression by Using Caged siRNAs with Single-Aptamer Modification, *Chembiochem*, 2018, **19**(12), 1259–1263.

25 H. Kappus and A. T. Diplock, Tolerance and safety of vitamin E: a toxicological position report, *Free Radic. Biol. Med.*, 1992, **13**(1), 55–74.

26 A. Rigotti, Absorption, transport, and tissue delivery of vitamin E, *Mol. Aspects Med.*, 2007, **28**(5–6), 423–436.

27 K. Nishina, *et al.*, Efficient In Vivo Delivery of siRNA to the Liver by Conjugation of α-Tocopherol, *Mol. Ther.*, 2008, **16**(4), 734–740.

28 Y. Uno, *et al.*, High-density lipoprotein facilitates in vivo delivery of α-tocopherol-conjugated short-interfering RNA to the brain, *Hum. Gene Ther.*, 2011, **22**(6), 711–719.

29 Y. Ji, *et al.*, Photochemical Regulation of Gene Expression Using Caged siRNAs with Single Terminal Vitamin E

Modification, *Angew Chem. Int. Ed. Engl.*, 2016, **55**(6), 2152–2156.

30 T. Nishina, *et al.*, Chimeric Antisense Oligonucleotide Conjugated to alpha-Tocopherol, *Mol. Ther. Nucleic Acids*, 2015, **4**, e220.

31 K. Nishina, *et al.*, DNA/RNA heteroduplex oligonucleotide for highly efficient gene silencing, *Nat. Commun.*, 2015, **6**, 7969.

32 E. Kilicay, *et al.*, In vitro evaluation of antisense oligonucleotide functionalized core-shell nanoparticles loaded with alpha-tocopherol succinate, *J. Biomater. Sci. Polym. Ed.*, 2017, **28**(15), 1762–1785.

33 B. T. Le, T. R. Kosbar and R. N. Veedu, Novel Disulfide-Bridged Bioresponsive Antisense Oligonucleotide Induces Efficient Splice Modulation in Muscle Myotubes in Vitro, *ACS Omega*, 2020, **5**(29), 18035–18039.

34 I. Ushach, *et al.*, Targeting TLR9 agonists to secondary lymphoid organs induces potent immune responses against HBV infection, *Mol. Ther. Nucleic Acids*, 2022, **27**, 1103–1115.

35 J. Soutschek, *et al.*, Therapeutic silencing of an endogenous gene by systemic administration of modified siRNAs, *Nature*, 2004, **432**(7014), 173–178.

36 C. Wolfrum, *et al.*, Mechanisms and optimization of in vivo delivery of lipophilic siRNAs, *Nat. Biotechnol.*, 2007, **25**(10), 1149–1157.

37 Y. Zheng and W. Tai, Insight into the siRNA transmembrane delivery—From cholesterol conjugating to tagging, *Wiley Interdiscip. Rev.:Nanomed. Nanobiotechnol.*, 2020, **12**(3), e1606.

38 G. Godard, *et al.*, Antisense effects of cholesterol-oligodeoxynucleotide conjugates associated with poly(alkylcyanoacrylate) nanoparticles, *Eur. J. Biochem.*, 1995, **232**(2), 404–410.

39 A. M. Krieg, *et al.*, Modification of antisense phosphodiester oligodeoxynucleotides by a 5' cholesteryl moiety increases cellular association and improves efficacy, *Proc. Natl. Acad. Sci. U. S. A.*, 1993, **90**(3), 1048–1052.

40 Y. K. Im, M. S. Kim and H. Yoo, Cholesterol conjugated spermine as a delivery modality of antisense oligonucleotide, *Int. J. Oral Myol.*, 2013, **38**(4), 155–160.

41 S. Wada, *et al.*, Evaluation of the effects of chemically different linkers on hepatic accumulations, cell tropism and gene silencing ability of cholesterol-conjugated antisense oligonucleotides, *J. Contr. Release*, 2016, **226**, 57–65.

42 M. Nakajima, *et al.*, Gene Silencing Activity and Hepatic Accumulation of Antisense Oligonucleotides Bearing Cholesterol-Conjugated Thiono Triester at the Gap Region, *Nucleic Acid Ther.*, 2017, **27**(4), 232–237.

43 F. Wada, *et al.*, Cholesterol-GalNAc Dual Conjugation Strategy for Reducing Renal Distribution of Antisense Oligonucleotides, *Nucleic Acid Ther.*, 2018, **28**(1), 50–57.

44 K. R. Kim, *et al.*, Cholesterol-Mediated Seeding of Protein Corona on DNA Nanostructures for Targeted Delivery of Oligonucleotide Therapeutics to Treat Liver Fibrosis, *ACS Nano*, 2022, **16**(5), 7331–7343.

45 M. Zuker, Mfold web server for nucleic acid folding and hybridization prediction, *Nucleic Acids Res.*, 2003, **31**(13), 3406–3415.

46 N. B. Justin Henri, J. Macdonald and S. Shigdar, A guide to using nucleic acid aptamers in cell based assays, *Aptamers*, 2019, **3**, 4–9.

47 E. M. Reyes-Reyes, Y. Teng and P. J. Bates, A new paradigm for aptamer therapeutic AS1411 action: uptake by macropinocytosis and its stimulation by a nucleolin-dependent mechanism, *Cancer Res.*, 2010, **70**(21), 8617–8629.

48 X. Li, *et al.*, Lipid-oligonucleotide conjugates for bioapplications, *Natl. Sci. Rev.*, 2020, **7**(12), 1933–1953.